

Self-coherent phase reference sharing for continuous-variable quantum key distribution

Adrien Marie^{1,*} and Romain Alléaume¹

¹Télécom ParisTech, LTCI, CNRS, 46 Rue Barrault, 75013 Paris, France

(Dated: May 2, 2022)

Generating "locally" the local oscillator is a fundamental requirement for continuous-variable quantum key distribution (CV-QKD), both for performance and security reasons. As a consequence, next-generation CV-QKD systems will have to be implemented with a local local oscillator (LLO). This issue has been explicitly tackled in recent works [1–3], where the proposed and implemented approach, that we call LLO-sequential, consists in sequentially (temporally) multiplexing quantum signal optical pulses with phase reference pilot tones optical pulses. We develop a comprehensive analysis of the noise model and the hardware requirements in order to perform LLO CV-QKD. This analysis allows to quantitatively understand one of the limits of CV-QKD implemented with the LLO-sequential approach: such systems, unless operated at very high speed, have very strong requirements in terms of tolerable laser phase noise. LLO-sequential CV-QKD can thus in practice only be implemented with expensive, low phase noise lasers, such as ECL lasers. Our model also allows to study the requirements in terms of amplitude modulation dynamics in order to jointly perform, with the same hardware, phase reference sharing and continuous-variable quantum communication. These elements indicate that the issue of developing a practical implementation of a fully functional CV-QKD system in LLO configuration remains an experimental challenge, especially with affordable hardware.

The main contribution of this work is to introduce LLO CV-QKD designs, experimentally implementable, to efficiently address this issue. We propose new designs based on self-coherence phase sharing, i.e. CV-QKD implemented with a local local oscillator, where the phase reference information and the quantum information are coherently obtained from a single optical wavefront produced by Alice laser. We propose in particular a design, called LLO-displacement, where the phase reference information is encoded in the displacement of the standard CV-QKD Gaussian modulated coherent state protocol. We analyze the performance and the hardware requirements of the LLO-displacement design. Our results clearly indicate that the LLO-displacement design can be used to perform CV-QKD for distances up to 100 km with realistic and affordable hardware, in particular with standard telecom equipment as low cost DFB lasers, opening a practical path towards the development of coherent quantum communications systems compatible with next-generation networks requirements.

I. INTRODUCTION

Quantum key distribution (QKD) [4, 5] is a promising technology that has reached the commercialization step since the last decade [6, 7]. Targeting deployment over large-scale networks, next-generation QKD should rely on affordable optical components. It will in particular consist in highly integrated systems able to operate at high rate and to be deployed over modern optical networks. Relying on standard telecommunication equipment, continuous-variable quantum key distribution (CV-QKD) is an attractive approach towards this new step of QKD development [8, 9]. While first results towards CV-QKD practical photonics chip integration have been pursued [10], the possibility to de effectively deploy CV-QKD in coexistence with intense wavelength-division multiplexing classical channels has been demonstrated [11]. Furthermore, high repetition rates (up to the order of hundreds of MHz) [12, 13] CV-QKD have also been implemented recently. More sensitive to optical losses than discrete-variable based QKD, long distance CV-QKD has however been demonstrated by controlling excess noise [14] and developing high efficiency error correction codes [15].

Practical implementations of CV-QKD rely on the use of coherent detections. These interferometric detections such as homodyne and heterodyne detections use a bright optical pulse, called local oscillator (LO). Coherent quadrature measurements depend on the relative phase between signal and LO pulses at interference. As such, the LO phase acts as a quadrature selector and an important requirement to allow information sharing between emitter and receiver is the phase coherence, i.e. a stable phase relation, between signal and LO. The issue of efficient phase reference sharing is thus a major issue in CV-QKD implementations. As the phase reference is an unspeakable information [16], it has to be optically encoded on a physical carrier. In classical coherent communication systems,

*Electronic address: adrien.marie@telecom-paristech.fr

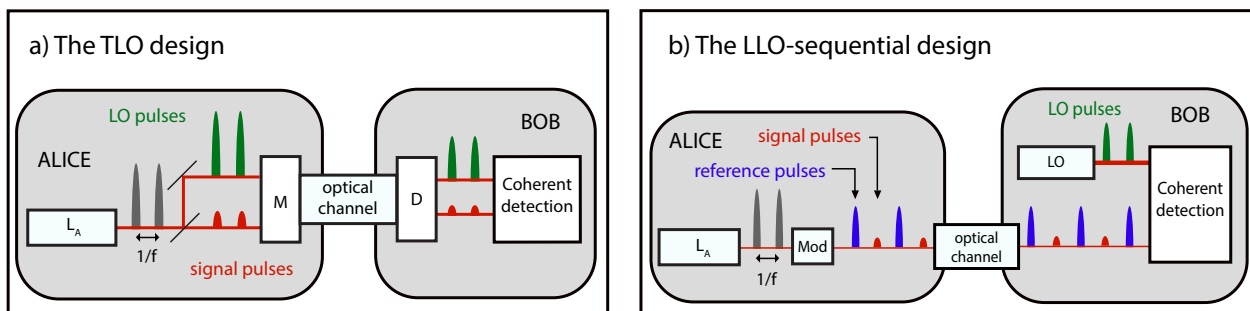


FIG. 1: (color) Experimental schemes of the TLO and LLO-sequential designs. *a)* Optical pulses are produced and split into signal and LO pulses. They are sent from Alice to Bob using multiplexing (*M*) and demultiplexing (*D*) techniques. Bob performs homodyne detection (*Hom*) using each signal/LO pair and recover information using digital signal processing (*DSP*). *b)* Alice sequentially sends signal and reference pulses to Bob. Using his local LO, Bob performs heterodyne detection (*Het*) in each pulse. Phase estimation (*Phase Est*) is performed on refence pulses allowing information recovering using *DSP*.

optical signals impinging on the detector typically contain a large number of photons while high bandwidth modulation and acquisition (typically 10 GHz or more) can be used. This has lead to tremendous progress in optical coherent communications in the past twenty years [17], relaxing the need to implement analog optical phase-lock loops between emitter laser and receiver local oscillator. Modern classical coherent communication systems, implementing for example the QPSK modulation format, can now be operated in a regime where the effective phase drift between consecutive pulses can be corrected using digital signal processing, based solely on optical quadrature measurement data.

Coherent quantum communication systems have on the other hand the constraints that they have to be use shot-noise limited detectors, i.e. detectors for which the electronic noise is not dominant over the shot noise. State-of the art shot-noise limited detectors remain so far limited to repetition rates below the GHz [13]. Moreover, the quantum signals sent by Alice cannot be of an intensity much larger than a few photons in order to ensure security in CV-QKD with realistic (below one) error correction efficiency [15]. As such, the phase sharing strategies used in classical coherent communication, that require a high number of photons at reception and high-speed modulations/detection cannot be directly applied to perform quantum coherent communications.

In most implementations of CV-QKD performed so far [13, 18–20], the phase reference is directly transmitted through the optical channel as a bright optical pulse multiplexed in time and polarization with each signal pulse and is used as the LO at reception. Such an implementation is detailed in Fig. 1.a) and is referred to as the Transmitted LO (TLO) design. The main advantage of this scheme is the simplicity of producing quantum signal and LO pulses pairs from a single laser placed at Alice. An interferometric set-up, based on polarization delay-line interferometers is used to multiplex (*M*) and demultiplex (*D*) the quantum signal and the LO, ensuring a low relative phase noise at reception. Security weaknesses of such implementations have however been demonstrated in practice by manipulating the LO intensity [21–23] or wavelength [24] on the quantum channel. Furthermore, the requirements on LO intensity at reception (around 10^8 photons per pulse at reception were required to ensure that the coherent detection can be operated with low electronic noise in [19]) create issues with respect to the coexistence of the LO with other signals propagating on the same optical channel. This will in particular limit the possibility of using the TLO scheme on shared optical fibers for long distance and high-rate operation, i.e. situations where the requirements on LO power at emission would be maximum.

In order to lift these important limitations on existing implementations relying on TLO, CV-QKD methods and demonstrations relying on a “local local oscillator” (LLO) have recently been introduced in [1–3]. One crucial advantage of implementing CV-QKD in a LLO configuration is to close, by design, any potential security loophole linked to the possibility of manipulating the LO as it propagates on the public optical channel between Alice and Bob. This is all the more important that LO manipulation attacks [21–24] constitute the main source of security loopholes identified so far in CV-QKD. Implementing LLO CV-QKD allows on the other hand to ensure by design that the LO is fully trusted, and in particular that the LO amplitude (that requires careful calibration) cannot be manipulated. Another important advantage of LLO CV-QKD stems from the fact that in this configuration, repetition rate and distance do not affect the LO intensity at reception. A LO power sufficient to ensure high shot-noise to electronic noise ratio may thus be obtained, independently of the propagation distance.

Implementing CV-QKD in the LLO configuration however comes with new experimental challenges. The main issue in LLO-based CV-QKD is to be able to perform CV-QKD despite the potentially important drift of the relative phase between Alice emitter laser and Bob local oscillator laser. The goal of phase reference sharing in the context

of CV-QKD is to allow Alice and Bob to share a reliable phase reference with a low enough phase noise in order to be able to exchange quantum information encoded on quantum states (coherent states modulated according to a bivariate Gaussian law in the case of the GMCS protocol [25]) so that the excess noise due to phase noise is significantly below the threshold imposed by the security proof [9]. Recent works [1–3] have demonstrated the possibility of implementing LLO-based CV-QKD method, with an experimental design that we will call LLO-sequential, depicted on Fig. 1.b). In the LLO-sequential design, Alice sequentially sends quantum signal and phase reference pulses at the repetition rate f . Phase reference pulses are relatively bright pulses compared to the signal and have a fixed phase in Alice phase reference frame, that is publicly known. At reception, Bob performs a coherent detection of both quantum signal pulses and phase reference pulses, using a single detector (heterodyne detector), operated with one “local local oscillator”, hence placed at Bob. The obtained quadrature measurement results, \hat{x} and \hat{p} , allow Bob to estimate the relative phase between Alice emitter laser and Bob local oscillator laser.

Based on the estimate $\hat{\theta}$, of the relative phase between Alice and Bob, Bob (respectively Alice) can locally perform a post-processing of the quadrature measurement data by performing a rotation of angle $-\hat{\theta}$. Both relative phase estimate and phase correction procedure can be implemented by digital signal processing (DSP). As demonstrated in [1, 2], LLO-sequential can be performed with moderate requirements in terms of reference pulse intensity (of the order of 10^3 photons) per pulse ; in particular phase reference intensity with the LLO-sequential design can be significantly below the required LO intensity in the TLO design (10^8 photons per pulse for MHz CV-QKD). LLO-sequential design can be in principle be implemented with existing technology and detector. In [2] a 250 kHz-clocked proof of principle experiment of the LLO-sequential designed is performed, however with only one single laser playing the role of both emitter and LO, and two consecutive uses of a homodyne detector used to emulate a heterodyne measurement. In [1], another proof-of-principle experiment with two lasers and Alice and Bob connected by a 25 km optical fiber is performed with a 50 MHz-clocked system. The authors demonstrate that phase correction can be implemented with a residual excess noise compatible with CV-QKD security threshold. Joint operation of CV-QKD together with the phase correction mechanism was studied through a simulation, which left aside the question of the requirements on the amplitude modulator dynamics in view of using the same modulator for both mechanisms. [3] provides a whole experimental demonstration of an implementation of LLO-sequential CV-QKD over 25 km, with a 100 MHz-clocked system, and a 1 GHz-bandwidth shot-noise limited homodyne detection. These strong experimental performances have been obtained with two low phase noise ECL lasers, as emitter and LO.

One crucial remark, in order to position the present work, is to notice that the LLO-sequential design has a fundamental limitation in its tolerance to high phase noise. Since the relative phase is evaluated on phase reference pulses emitted $\frac{1}{f}$ seconds before (or after) the actual quantum signal pulses, the precision with which the relative phase (between Alice laser and Bob laser) can be evaluated *on the actual quantum signals* is intrinsically limited to a quantity scaling as $\sim \frac{\Delta\nu}{f}$ where $\Delta\nu$, quantifies the laser phase noise and f is the repetition rate. As we will see in the next section, the effective phase noise can be effectively related, under a standard assumption of the phase noise model, to the linewidths of Alice, respectively Bob lasers ($\Delta\nu_A, \Delta\nu_B$). Current bandwidth limitation of shot-noise limited coherent detectors currently impose to choose f below 100 MHz. This imposes in return strong requirements on the phase noise of the lasers that can be used in order to perform LLO-sequential CV-QKD: the linewidth of the laser must be well below 100 MHz. As a consequence, only very low phase noise lasers, such as external-cavity lasers (ECL), whose typical spectral linewidth is of a few kHz, are typically needed to implement LLO-sequential design, as illustrated with the experimental choices of ECL lasers with 1.9 kHz linewidth in [3], while narrow line lasers locked to a frequency standard where used in [2].

In this work, we propose practical designs for LLO CV-QKD based on the idea of self-coherence (SC) phase reference sharing schemes. SC designs consist in ensuring physical coherence between signal and phase reference by deriving both of them from the same optical source pulse. We also introduce two experimental designs respectively based on the displacement of Alice’s modulation, said LLO-displacement design, and on delayed reference pulses, said LLO-delayline, both implementing self-coherent phase reference sharing CV-QKD. Based on these two designs, we show that self-coherence phase sharing allows to work in high phase noise regime using realistic experiment hardware, and in particular that it can be implemented with existing shot-noise limited detector, even with moderate bandwidth (tens of MHz) together with low cost distributed feedback (DFB) lasers whose typical linewidth is in the lower MHz range.

In Table I, we summarize the characteristics of existing as well as newly proposed designs for CV-QKD, the latter being described in more details in Section III. The two major advantages of LLO CV-QKD are the fact that the LO can be fully trusted LO and the fact that it relaxes implementation constraints associated with LO transmission and multiplexing (in particular the interferometric design associated with TLO). The main challenge of LLO CV-QKD is however that the phase drift between emitter laser and local oscillator laser, placed at Bob, induces a phase noise on the quantum communication, that has to be efficiently corrected. As explained above, the LLO-sequential design

Exp. design	Advantages	Drawbacks
Transmitted LO (Fig. 1.a) [13, 18–20]	Limited phase noise by design No time multiplexing	Security issues LO intensity at reception LO transmission Experimental complexity (interferometer)
LLO-sequential (Fig. 1.b) [1–3]	LO fully trusted	Strong requirements on phase noise Constraints on AM dynamics Constraints on detector linearity
LLO-displacement Sec. III A	LO fully trusted Can be operated even with high phase noise No time multiplexing	Constraints on AM dynamics Constraints on detector linearity
LLO-delayline-dsp Sec. III C 2	LO fully trusted Can be operated even with high phase noise	Constraints on AM dynamics Constraints on detector linearity Experimental complexity
LLO-delayline-opll Sec. III C 3	LO fully trusted Limited phase noise by design	Constraints on AM dynamics Two coherent receivers Experimental complexity (interferometer)

TABLE I: Summary of the different CV-QKD designs considered in this work.

is intrinsically limited to low phase noise regimes, i.e. regimes where the relative phase drift at the timescale $\frac{1}{f}$ is much smaller than 2π . This puts important constraints on the type of lasers that can be used both as emitter and LO. We propose in this work new LLO designs allowing to obtain a stronger tolerance to phase noise based on the idea of self-coherence between quantum signal and phase reference. Our LLO-displacement design is based on the encoding of phase reference information into the displacement of Alice GMCS modulation. Since both quantum signal and phase reference information are sent over the same optical pulse, the key rate obtained with the LLO-displacement design is moreover not lowered by time multiplexing, as it is the case with LLO-sequential. The two LLO-delayline designs can be seen as the translation of the multiplexing idea used in the transmitted LO (TLO) design, in order to obtain self-coherent LLO implementations. They rely on balanced delayline interferometers placed at the emitter and receiver side, implying some additional experimental complexity.

In order to compare the global performance of those designs, a comprehensive noise model taking into account LLO experimental issues is introduced in Sec. II. The LLO-displacement and LLO-delayline designs are then introduced in Sec. III and compared from a realistic viewpoint. Conclusion and perspectives are presented in Sec. IV.

II. COMPREHENSIVE NOISE MODEL FOR PHASE SHARING PERFORMANCE ANALYSIS

In order to compare the different experimental CV-QKD designs of this work in terms of secret key rate, we here introduce the notations and the noise model we consider throughout this paper. First, we briefly recall the Gaussian-modulated coherent state protocol and the standard excess noise sources in CV-QKD analysis. We then justify and introduce new elements in the noise model in order to allow the analysis of LLO-based CV-QKD more precisely in realistic hardware regimes.

The GMCS protocol. In this work, we focus on the Gaussian modulated coherent state (GMCS) CV-QKD protocol [25]. This protocol runs as follows: at cycle i , Alice encodes classical zero-mean Gaussian variables $(x_A^{(i)}, p_A^{(i)})$ of variance V_A on the two conjugate quadratures of a coherent state $|\alpha_i\rangle = |x_A^{(i)}, p_A^{(i)}\rangle$. The consecutive coherent states $|\alpha_i\rangle$ are sent to Bob at the repetition rate f through an insecure optical channel controlled by an eavesdropper Eve. For simplicity, we do not consider the time domain in this section and derive equations for only one cycle with coherent state $|\alpha\rangle$. At reception, Bob performs a homodyne detection of a randomly chosen quadrature on each coherent state $|\alpha\rangle$. After processing, Bob gets classical measurement outcome x_B or (p_B) which is an estimation of Alice's input. In this work, we consider reverse reconciliation. Furthermore, we assume that Eve's behavior is captured under the collective model attacks [26]. As the optimal attack is Gaussian, the communication channel between classical variables (x_A, p_A) and (x_B, p_B) is modeled as a Gaussian channel which can be written as:

$$x_B = \sqrt{G} \cdot (x_A + x_0 + x_C) \quad (1)$$

where G is the total channel intensity transmission, x_0 is the shot noise of variance 1 and x_C is the total noise of

variance χ referred to Alice. We can express the variance χ of x_c as:

$$\chi = \frac{1-G}{G} + \xi \quad (2)$$

which is the sum of the loss-induced noise $1/G - 1$ and the channel excess noise ξ . As such, the Gaussian channel is fully characterized by G and ξ and the secret key rate is fully determined by these two parameters using the equations [27] described in Annex VA. We have here only considered homodyne detections but in the next we introduce experimental designs relying on heterodyne detections. Heterodyne detections are phase diversity homodyne detection. Both coherent state quadratures are measured but an extra shot noise is added to the excess noise due to quantum signal split. Specific secret key rate formulas for heterodyne receiver are also detailed in Annex VA.

Noise model of our analysis. In order to compare the different designs, we discuss the different excess noise sources contributing in the excess noise ξ .

- *Electronic to shot noise ratio.* Electronic noise of Bob's detector induces a noise of variance v_{elec} on Bob's quadrature measurements in shot noise unit (SNU). In general, the electronic noise variance v_{elec} depends on the detection circuit as well as on the repetition rate of the experiment. As the shot noise value scales with the LO intensity, it is however possible to reduce the effective electronic to shot noise ξ_{elec} impact by increasing the LO intensity. We express ξ_{elec} referred to Alice in SNU as:

$$\xi_{\text{elec}} = \frac{\delta_{\text{det}}}{G} \cdot \frac{E_{\text{LO,cal}}^2 \cdot v_{\text{elec}}}{E_{\text{LO}}^2} \quad (3)$$

where $E_{\text{LO,cal}}^2$ is the photon number in the LO at which $\xi_{\text{elec}} = v_{\text{elec}}$ and E_{LO}^2 is the photon number per LO pulse at reception. The variable δ_{det} stands for the detection method as $\delta_{\text{det}} = 1$ for a homodyne receiver and $\delta_{\text{det}} = 2$ for a heterodyne receiver. In general, the variance v_{elec} increases with the repetition rate, for a given detection circuit. For instance, in [18], the same detector has an electronic to shot noise ratio of -6 dB at 50 MHz, -4 dB at 200 MHz and -1 dB at 1 GHz. In the following, we consider an average electronic to shot noise ratio v_{elec} of -4 dB for $N_{\text{LO,cal}} = 10^8$ photons per LO pulse independently of the repetition rate. Furthermore, we consider the electronic noise as fully trusted which corresponds to a realistic model [2].

- *Limitation on the launch power at Alice's side.* In the following, we note E_{in}^2 the mean number of photons in each pulse produced by L_A at Alice's side:

$$E_{\text{in}} = \sqrt{\tau \cdot I_{\text{laser}} \cdot \frac{\lambda}{hc}} \quad (4)$$

where τ is the pulse duration (we use $\tau = 0.1/f$), $\lambda = 1550$ nm, h the Planck constant, c the speed of light and I_{laser} is Alice's laser intensity. Throughout this paper, we refer to E_{in} as an amplitude which is the square root of a photon number and is homogeneous in dimension to a coherent state quadrature. Because of limited power of lasers as well as Brillouin effect and other non-linear effects in optical fibers [28–30], there is a limit I_{max} of few tens of milliwatts on the launched power I_{laser} of each involved laser for CV-QKD purposes which depends on the coherence of lasers, the optical fiber or presence of shared signals in the fiber. In the TLO design, this limit I_{max} is a major limitation of the LO intensity at reception, especially for long distances, because it increases the electronic noise impact according to Eq. 3. The local LO of LLO designs fixes this limitation.

- *Relative phase noise.* We here consider the excess noise due to the relative phase drift between signal and local oscillator pulses. In the GMCS protocol, Alice sends consecutive coherent states $|\alpha\rangle$ to Bob at a repetition rate f . In quantum optics, quadratures of an optical mode are always referred to a phase reference and a natural reference frame is the free-running phase of the source laser. As such, Alice encodes Gaussian variables (x_A, p_A) on the quadratures of coherent state $|\alpha\rangle$ produced by laser L_A which is then written in Alice's reference frame as:

$$|\alpha\rangle = x_A + i \cdot p_A = E \cdot \exp(i \cdot \theta_{\text{state}}) \quad (5)$$

At reception, Bob performs a homodyne detection of $|\alpha\rangle$ which is an interferometric detection relying on a strong phase reference coherent state $|\beta\rangle$, the local oscillator (LO). From a theoretical point of view, a homodyne detection can be seen in the phase space as the projection of the coherent state $|\alpha\rangle$ on the quadrature corresponding

to phase of the LO. In Alice's reference frame, the state $|\beta\rangle$ has a phase θ which is the relative phase between Alice's reference frame and the LO. The relative phase θ thus acts as the selector of measured quadrature. The outcome x_B of the \hat{x} quadrature measurement of state $|\alpha\rangle$ can be written as:

$$x_B = x_A \cos \theta - p_A \sin \theta + x_0 + x_C \quad (6)$$

which corresponds to Eq. 1 in presence of a relative phase θ and where $G = 1$ for simplicity. In general, the relative phase θ is a random variable. Considering the time structure of the protocol, successive coherent states $|\alpha_i\rangle$ interferes with LO pulses $|\beta_i\rangle$ at cycle i at a repetition rate f . We model the relative phase over time at interference as a Gaussian stochastic process $(\theta_i)_i$ expressed as:

$$\theta_{i+1} = \theta_i + \delta\theta_i \quad (7)$$

where $\delta\theta_i \sim \mathcal{N}(0, V_{\text{drift}})$ where V_{drift} is the relative phase drift during a time interval of length $1/f$. As shown in Eq. 6, the random relative phase drift acts as a decorrelation process between Alice's variables and Bob's measurements and, as such, has to be corrected. Based on an estimate $\hat{\theta}$, calculated at reception, of the relative phase noise θ , phase correction can be applied on Alice and Bob's data in order to decrease the induced excess noise. In reverse reconciliation, Bob sends his estimate to Alice which performs a phase drift correction (rotation of her variables). We call phase noise the variance $V_{\hat{\theta}}$ of θ given the estimate $\hat{\theta}$. The excess noise induced by the relative phase noise can be written, for a zero-mean GMCS modulation as (derivations of this calculation are detailed in Annex. VB 1):

$$\xi_{\text{phase}} = GV_A \cdot (1 - e^{-V_{\hat{\theta}}}) \quad (8)$$

In the TLO design, both quantum signal and LO pulses are produced with laser L_A at emission ensuring a strong ad-hoc physical phase coherence at interference because the relative phase θ is directly 0. Furthermore, the relative phase drift V_{drift} only comes from low frequency fluctuations of the different optical paths (Fig. 1.a) and is close to 0. In TLO implementations, the low phase noise is efficiently corrected using post-processing algorithms.

In the LLO-sequential design however, the LO pulses $|\beta_i\rangle$ are produced by Bob's laser L_B (Fig. 1.b) and the relative phase drift is then dominated by the fast relative phase drift between L_A and L_B . In particular, the phase θ_i at interference is a priori fully random and x_A and x_B are decorrelated. However, using an estimate of the relative phase, a post-processing can restore correlations from Bob's measurement outcomes. In the LLO-sequential design, Alice sends pulses pairs $(|\alpha_{2k}\rangle, |\alpha_{2k+1}\rangle)$ where $|\alpha_{2k}\rangle$ is the quantum signal defined in Eq. 5 and $|\alpha_{2k+1}\rangle = |E_{\text{ref}}\rangle$ is a phase reference pulse with a fixed phase set to 0 and an amplitude E_{ref} . Measuring both quadratures of the reference pulse, Bob can calculate an estimate $\hat{\theta}_{2k+1}$ of the relative phase θ_{2k+1} as:

$$\hat{\theta}_{2k+1} = \tan^{-1} \left(\frac{p_B^{(2k+1)}}{x_B^{(2k+1)}} \right) \quad (9)$$

where $(p_B^{(2k+1)}, x_B^{(2k+1)})$ are Bob's measurement outcomes. We can write the variance V_M of $\hat{\theta}_{2k+1}$ as:

$$V_M = \frac{2}{G \cdot E_{\text{ref}}^2} \quad (10)$$

This shows that a large amplitude E_{ref} allows to recover the relative phase with high sensitivity. Thus, Bob uses the estimate $\hat{\theta}_{2k+1}$ to correct the outcomes of $|\alpha_{2k}\rangle$ measurement. However, in this case, the relative phase drift depends on the spectral linewidths $\Delta\nu_A$ and $\Delta\nu_B$ of respectively lasers L_A and L_B and is expressed as:

$$V_{\text{drift}} = \text{var}(\theta_{i+1}|\theta_i) = \frac{2\pi \cdot (\Delta\nu_A + \Delta\nu_B)}{f} \quad (11)$$

Finally, Bob estimates the relative phase at quantum signal $|\alpha_{2k}\rangle$ interference with a remaining phase noise of variance $V_{\hat{\theta}}$:

$$V_{\hat{\theta}} = \text{var}(\theta_{2k}|\hat{\theta}_{2k+1}) = V_M + V_{\text{drift}} \quad (12)$$

From Eq. 12, we shown that the remaining phase noise variance at least the variance V_{drift} of the relative phase drift between two consecutive pulses. We emphasize that this noise can not be corrected and thus intrinsically restricts the use of the LLO-sequential designs in experimental regimes where $V_{\text{drift}} \ll 1$. From a experimental point of view, this corresponds to very stable but expensive ECL use or high repetition rates regimes requiring low noise

high-speed coherent detectors. In the LLO-sequential analysis, we consider heterodyne detection of the reference pulses. As shown in [2], a homodyne detection can be used if Alice send pairs of reference pulses instead of only one.

Need of a refined model for LLO-based phase sharing designs performance analysis. We here introduce new elements in the noise model and then justify their necessity in the analysis of LLO-based CV-QKD performance.

Amplitude modulator imperfections model. The LLO-implementation design requires to modulate relatively intense phase reference pulses as well as shot-noise limited quantum signals. In integration and experimental simplicity perspectives, we consider that those pulses are produced using the same amplitude modulator (AM). This directly addresses the issue of the AM dynamics at emission. We here introduce an analytic model describing amplitude modulator imperfections. In practice, an AM is a Mach-Zehnder interferometer [31] with a phase modulator controlling the relative phase of the two arms. This relative phase ψ_0 defines the amplitude transmission of the AM and we can write:

$$E = E_{\text{in}} \cdot \cos \frac{\psi_0}{2} \quad (13)$$

where E_{in} is the amplitude of the incoming field from Eq. 4 and $E \leq E_{\text{in}}$ is the amplitude of the coherent state to be modulated. However, due to finite modulation dynamics of the phase modulator, the exact applied phase is written as $\psi_0 + \delta\varphi$ where $\delta\varphi \sim \mathcal{N}(0, V_\varphi)$. Thus, the produced amplitude E' is written as $E' = E_{\text{in}} \cdot \cos \left(\frac{\psi_0 + \delta\varphi}{2} \right)$. If $V_\varphi \ll 1$, we can write E' as:

$$E' \approx E + \frac{\delta\varphi}{2} \sqrt{E_{\text{in}}^2 - E^2} \quad (14)$$

Then, such AM imperfections introduce a leakage on the amplitude modulation introducing errors on the communication channel. Furthermore, Eq. 14 shows that the leakage increases with the incoming amplitude E_{in} . More particularly, the expectation value of the leakage increases with the difference $E_{\text{in}}^2 - \langle E \rangle^2$ where $\langle E \rangle$ is the expectation value of E over Alice's modulation (for instance, the Rayleigh distribution of the amplitude in case of zero-mean Gaussian modulation of TLO results in $\langle E \rangle = \sqrt{\pi V_A/2}$). Thus, the amplitude E_{in} should be chosen as close to $\langle E \rangle$ as possible. However, as the amplitude E_{in} is the maximal amplitude that Alice can produce, it also can be seen as a truncation of Alice's modulation amplitude. As demonstrated in [32], this inevitable experimental truncation must occur at least few times the standard deviation $\sqrt{V_A}$ from the expectation $\langle E \rangle$ and should be as larger than $\langle E \rangle$ than possible. These two effects finally lead to a trade-off and an optimisation of the amplitude E_{in} depending on the distribution of the signal amplitude distribution.

We also relate the introduced variance V_φ to the well-known dynamics of the modulator, denoted dyn_{dB} , by writing the minimal and maximal amplitudes $E_{\text{min}} \approx \delta\varphi E_{\text{in}}$ and $E_{\text{max}} \approx E_{\text{in}}$ the modulator can output and using the definition of the dynamics dyn_{dB} :

$$\text{dyn}_{\text{dB}} = 10 \cdot \log_{10} \left(\frac{E_{\text{max}}}{E_{\text{min}}} \right) = 10 \cdot \log_{10} \left(\frac{1}{V_\varphi} \right) \quad (15)$$

Linearity range of the detection. For practical simplicity, we also consider that only one coherent detector is used to detect both quantum signals and reference pulses. This addresses the issue of the linearity range of the detector. A typical homodyne detector is presented in Fig. 2. In practice, the response of the integrator circuit is proportional to the incoming number of electrons over a finite range. Beyond a threshold, which depends on the circuit, the response of the integrator circuit is not linear and the security can be broken by specific attacks [33]. In this work, we define this threshold as the maximal number of electrons N_{sat} per electrical pulses that can be detected in a linear regime. For perfect intensity transmission, the number of electrons in each electrical pulse is $N_e = E_S \cdot E_{\text{LO}}$ where E_S and E_{LO} are the amplitudes of the signal and the LO so that the saturation hypothesis imposes:

$$E_S \cdot E_{\text{LO}} \leq N_{\text{sat}} \quad (16)$$

The saturation threshold N_{sat} can then be experimentally measured by increasing the amplitude of the signal up to the saturation of the detector. The value $N_{\text{sat}} = 10^6$ has then been evaluated in [33]. For quantum signal of intensity of order of the shot noise, this threshold is not important and has not been considered so far in CV-QKD analysis. In LLO-based CV-QKD however, the relatively large amplitude of phase reference pulses imposes to consider the saturation threshold as a limit on the reference pulses amplitude. In order to increase the maximal

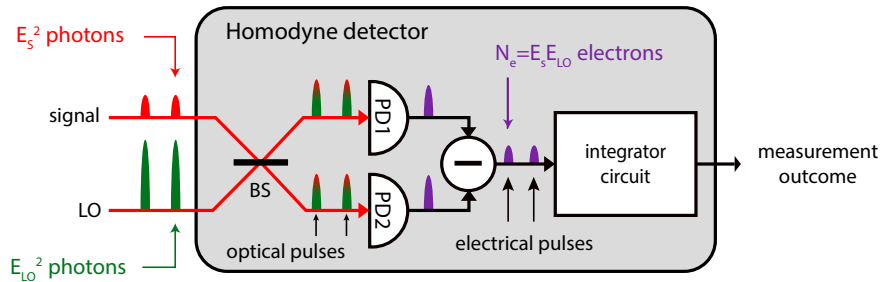


FIG. 2: (color) Scheme of a typical homodyne detector. Signal and local oscillator pulsesw interfere on a 50/50 beamsplitter (BS). Both resulting fields are detected on two photodiodes (PD1 and PD2) which convert photons into electrons. The electrical pulses (purple pulses) produced by the photodiodes are then subtracted (-) and the resulting quadrature electrical pulse intensity is measured using an integrator circuit. The outcome of the integrator circuit is proportinnal to $N_e = E_s \cdot E_{LO}$ up to an intensity threshold N_{sat} .

reference pulse amplitude, the LO intensity can also be reduced resulting on a increased electronic to shot noise ratio (Eq. 3). Finally, the finite linearity range of the detector leads to a trade-off between the phase reference amplitude and the electronic to shot nosie ratio.

Discretization of Bob's digital acquisition. The requirement of relatively bright reference pulse increase the range of the quadrature measurements. As the finite number of bits d_{acq} of Bob's acquisition data card discretizes the values of the measurements, the excess noise due to this discretization is larger when refrence pulses are considered. This excess noise is written as:

$$\xi_{disc} = \frac{E_{in}^2}{2^{2d_{acq}}} \quad (17)$$

referred to Alice. As a local noise on Bob's receiver, this noise behaves as the electronic noise and can be trusted in realistic regimes. Furthermore, as shown in the next, optimal values of E_{in}^2 are of order of 10^4 photons and d_{acq} is usually at least 12 bits resulting in $\xi_{disc} \leq 10^{-4} N_0$ which is not significant in noise analysis.

We have shown that the requirement of specific phase reference pulses with relatively bright amplitudes in LLO methods addresses practical issues. The ability of simultaneously exchanging quantum signals and bright reference pulses using only one experimental setup is limited by the finite AM dynamics as well as by the linearity range of the detection. These effects are not considered in TLO designs because only weak quantum signals are modulated and detected but they are key parameters in order to compare realistic implementations of LLO-based CV-QKD in terms of secret key rate. To our knowledge, the amplitude modulator and linearity range issues have not been taken into account so far in CV-QKD analysis. Based on this refined model, we now introduce two new designs, LLO-displacement and LLO-delayline, and analyze their performances.

III. SELF-COHERENCE IN PHASE REFERENCE SHARING

Strong performance limitations of the LLO-sequential design come from the time delay between signal and phase reference pulses emissions and impose to work at low phase noise regimes. In this section, in contrast of sequential phase and reference pulse generation, we introduce the idea of self-coherent (sc) phase reference sharing for LLO-based CV-QKD. Self-coherent designs consist in ensuring the physical coherence between signal and phase reference by deriving both of them from the same optical pulse at emission. Doing this, the relative phase between signal and phase reference is not affected by the relative phase drift of the lasers and the phase correction can be performed with high sensivity even in high phase noise regimes. In the following, we propose two self-coherent LLO designs and discuss their performance using the noise model introduced in Sec II.

A. Description of the LLO-displacement design

We propose a first design to perform CV-QKD with a self-coherent phase reference sharing. In this LLO-displacement design both quantum signal and phase reference information are encoded jointly over the each

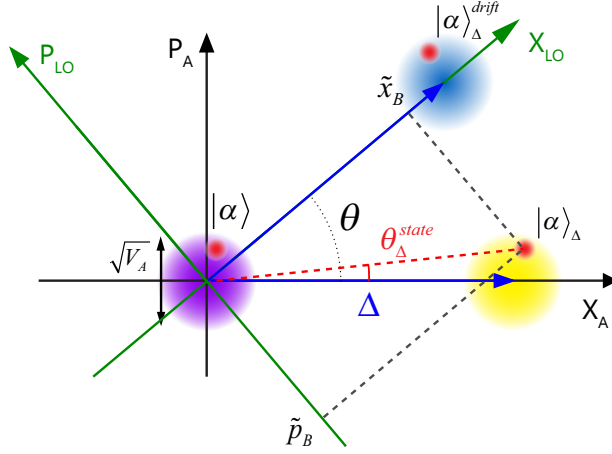


FIG. 3: (color) Phase space representation of Alice's thermal state. The (purple) centered circle represents the zero-mean variance V_A modulation of both TLO and LLO-sequential designs signal. The (yellow) right circle represents the displaced modulation in the LLO-inband design referred to Alice's phase reference. The displacement Δ corresponds to the phase reference. The (blue) top circle is Alice's modulation from Bob's point of view. Due to phase noise, Alice's thermal state is rotated by a random phase θ_{drift} . In the regime where $\Delta \gg \sqrt{V_A}$, the phase θ_{state} is close to 0 which allows Bob to efficiently estimate the phase drift θ_{drift} . This scheme is valid for $G = 1$.

optical pulse produced by Alice's laser L_A at emission. We show that this scheme can be highly resilient to phase noise using realistic parameters.

Description of the design. The idea is to implement the GMCS protocol but to displace the coherent state constellation (corresponding to a thermal state) sent by Alice by a displacement Δ of phase ϕ_Δ as represented in Fig. 3. Instead of sending $|\alpha\rangle = |x_A, p_A\rangle$ (centered (green) modulation in Fig. 3), Alice sends the displaced coherent state $|\alpha\rangle_{\Delta} = |x_A + \Delta \cos \phi_\Delta, p_A + \Delta \sin \phi_\Delta\rangle$, with x_A and p_A her Gaussian variables. Without loss of generality, ϕ_Δ can be set to 0 and the displaced coherent state (right (yellow) modulation in Fig. 3) is then:

$$|\alpha\rangle_{\Delta} = |x_A + \Delta, p_A\rangle = |E \cdot e^{i\theta_{\Delta}^{\text{state}}}\rangle \quad (18)$$

The amplitude of the displacement is publicly known and its phase is fixed to 0 in Alice's reference frame so that it carries information on her phase reference. At reception, Bob measures both \tilde{x} and \tilde{p} quadratures of each received coherent state $|\alpha\rangle_{\Delta}$ using a heterodyne detection and gets measurement outcomes $(\tilde{x}_B, \tilde{p}_B)$ as represented in Fig. 3. From these measurements, Bob can estimate the relative phase θ with an estimator $\hat{\theta}$ using the formula from Eq. 9. This estimator is actually an estimation of the phase $\theta - \theta_{\Delta}^{\text{state}}$ but the standard deviation of $\theta_{\Delta}^{\text{state}}$ over Alice's modulation is small when Δ is large. We can write the variance of $\hat{\theta}$ as:

$$V_M = \frac{GV_A + 2}{G\Delta^2} \quad (19)$$

and we refer to V_M as the single phase estimation. We emphasize that the remaining phase noise is then, at most, the variance V_M . In particular, it does not depend on the phase drift V_{drift} between two consecutive pulses. After post-processing, Bob estimates Alice's quadratures with the following (x_B, p_B) :

$$(x_B, p_B) = R_{\hat{\theta}}(\tilde{x}_B, \tilde{p}_B) - (\Delta, 0) \quad (20)$$

where $R_\theta(P)$ is a rotation of the point P of angle θ in \mathbb{R}^2 . As signal and phase reference are transmitted on the same optical pulse using a displacement of the mean amplitude, we will refer to this design as LLO-displacement. The experimental setup is described in Fig. 4.

Collective phase estimation with LLO-displacement design. From Eq. 19, we can see that provided that Δ is large, Bob has a precise estimation of the relative phase using single state quadrature measurements. However, using the Gaussian phase noise structure from Eq. 7, the efficiency of the phase estimation process can be optimized by using consecutive phase estimations. Basically, the idea of collective phase estimation is to use time phase correlations by averaging adjacent phase estimations over a window of many estimations. The optimal size of this

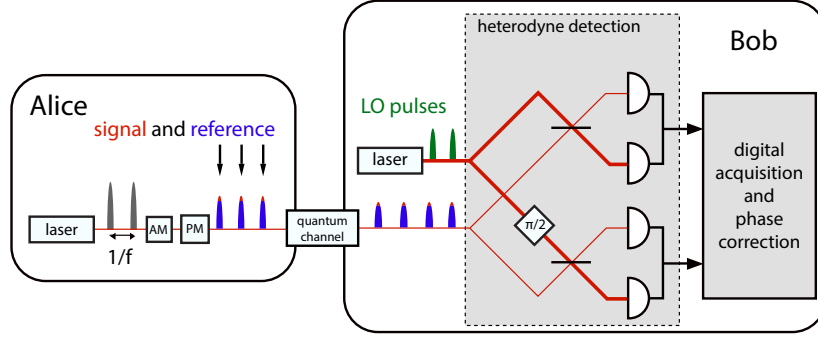


FIG. 4: (color) Experimental scheme of the LLO-displacement design. Signal and phase reference are both encoded on the same optical pulse using the modulation of Fig. 3. At reception, Bob performs heterodyne detection on every pulse using his own laser as LO (green pulses) and can both evaluate the phase drift and correct his quadrature measurements.

window depends on the variance V_{drift} as well as on the variance V_M of Eq. 19. Finally, we can write the optimal phase estimation variance $V_{\hat{\theta}}$ as:

$$V_{\hat{\theta}} = \frac{V_M}{n_{\text{opt}} + 1} + \frac{V_{\text{drift}}}{6} \cdot \frac{n_{\text{opt}}(2n_{\text{opt}} + 1)}{n_{\text{opt}} + 1} \quad (21)$$

where $n_{\text{opt}} + 1$ is the optimal size of the filtering window and can be written as:

$$n_{\text{opt}} = \left\lfloor \frac{\sqrt{V_{\text{drift}} + 6V_M}}{\sqrt{2V_{\text{drift}}}} \right\rfloor \quad (22)$$

For instance, in low phase noise regimes ie. where $V_{\text{drift}} \ll 1$, adjacent estimations can be averaged to increase the overall phase estimation efficiency. However, in high phase noises regime where $V_{\text{drift}} \gg V_M$, Eq. 22 leads to $n_{\text{opt}} = 0$ and the estimation process efficiency is directly the single measurement based efficiency and $V_{\hat{\theta}} = V_M$. In particular, this means that even in case of strong phase noise, the relative phase can be recovered with precision at least V_M using the displacement Δ . We can write the excess noise due to the phase noise as:

$$\xi_{\text{phase}}^{\text{disp}} = 2V_A \cdot (1 - e^{-V_{\hat{\theta}}}) + \Delta^2 \cdot \left(\frac{1}{2} + \frac{1}{2} e^{-2V_{\hat{\theta}}} - e^{-V_{\hat{\theta}}} \right) \quad (23)$$

The derivation of the $\xi_{\text{phase}}^{\text{disp}}$ formula is detailed in Annex VB 1. We can show that the $\xi_{\text{phase}}^{\text{disp}}$ decreases as Δ increases and thus that the phase recovery process requires a displacement as large as possible. Unlike in the LLO-sequential design in which the relative phase is estimated from adjacent pulses, the relative phase is now estimated using collective estimation that includes self-coherent reference. This implies that even if the phase noise is high and the relative phase is totally decorrelated from a pulse to the following one, Bob can still get information on the relative phase and correct his measurements. In particular, the LLO-displacement design allows to perform CV-QKD in the regime of large phase noise which can not be achieved using the LLO-sequential design. Furthermore, this phase reference transmission method directly saves a factor 2 in the key rate formulas compared to previously introduced LLO-based designs since all pulses contribute to quantum communication at repetition rate f .

Amplitude modulator imperfections and finite linearity range limit the displacement amplitude. The phase estimation scheme requires a large displacement to be efficient. In practice however, the displacement amplitude is limited by the AM leakage that we have modelled in Eq. 14. A trade-off needs to be made between the phase estimation efficiency and the modulator induced excess noise. We can derive the excess noise due to amplitude modulation as:

$$\xi_{\text{mod}} = \frac{V_{\varphi}}{8} (E_{\text{in}}^2 - \Delta^2) + \frac{\Delta^2 + 2V_A}{2} \left(\frac{1}{1 + \frac{\Delta^2}{V_A}} + 1 \right) \exp \left[-\frac{(\Delta - E_{\text{in}})^2}{2V_A} \right] \quad (24)$$

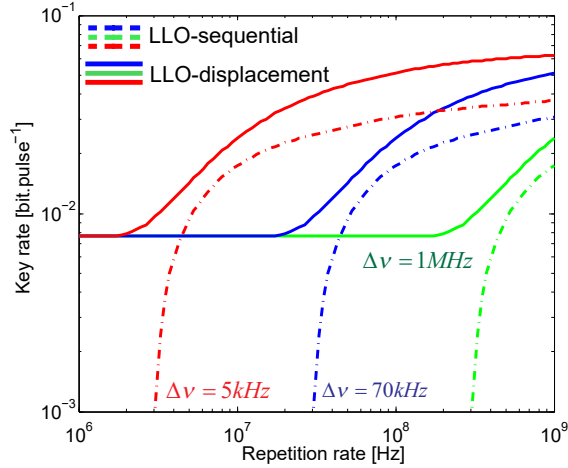


FIG. 5: (color) Comparison of the theoretical expected key rates of LLO-displacement and LLO-sequential for $\Delta\nu$ equal to 5 kHz, 70 kHz and 1 MHz. Dashed curves correspond to the LLO-sequential and solid curves to LLO-displacement. In this figure, we have set the AM dynamics at 30 dB.

The first term corresponds to the AM noise of Eq. 14. These fluctuations impose that E_{in} should not be much larger than Δ . The second term of Eq. 24 corresponds to the truncation of the modulation and imposes that the difference $E_{\text{in}} - \Delta$ has to be larger than $\sqrt{V_A}$. Then, these two behaviors impose an optimal E_{in} .

B. Performance analysis of the LLO-displacement design

In this section, we study the LLO-displacement design in terms of secret key rate and compare its performances to the LLO-sequential design based on theoretical simulations. We first discuss our simulation model an hypothesis.

Simulation hypothesis. In this paragraph, we detail our simulation settings. We first detail parameters which are fixed throughout this paper. The reconciliation algorithm efficiency is set to $\beta = 0.95$ and the photodiodes efficiency to $\eta = 0.7$. The finite number of acquisition bits d_{acq} is chosen to 12 bits which is compatible with standard acquisition cards. We consider $\alpha = 0.2 \text{ dB.km}^{-1}$ loss optical fibers. The electronic to shot noise ratio is set to -4 dB , which corresponds to $\xi_{\text{elec}} = 0.39 \text{ SNU}$. Finally, a systematic system noise $\xi_{\text{tech}} = 0.01 \text{ SNU}$ is always considered. Furthermore, important parameters in our analysis are the spectral linewidth of the involved lasers and the AM dynamics at emission. We consider that the more stable lasers compatible with CV-QKD experiments are external-cavity lasers (ECL) for which the linewidth $\Delta\nu$ is of order of few kHz (typically 5 kHz). On the opposite, standard distributed feedback (DFB) lasers have typical spectral linewidths three orders of magnitude above, around few 1 MHz. Standard AM dynamics dyn_{dB} are of order of few tens of dB. In this work, we consider AM dynamics from 15 dB for low cost AM up to 60 dB for performant modulators. Our choices in terms of all these parameters are motivated by standard values compatible with experimental implementations.

Furthermore, our analysis imposes optimization constraints for some parameters. The modulation variance V_A is an important parameter which has an optimal value depending on the distance d and on the parameter β [15] and, in our case, of the displacement Δ . As shown in Fig. 24, a trade-off in term of E_{in} has to be done between AM dynamics induced excess noise and the truncation of Alice's modulation. We have also shown in Eq. 16 that the finite linearity range, fixed to $N_{\text{sat}} = 10^6$ photons, imposes a practical limit on the product of the quantum signal, which is essentially determined by the displacement Δ (or E_{ref} for the LLO-sequential design), and the LO amplitudes which constraints the value ξ_{elec} . In all our simulations, the values V_A , E_{in} and Δ are chosen to optimize the secret key rate while the LO amplitude is chosen as $E_{\text{LO}} = N_{\text{sat}} / \sqrt{\eta T E_{\text{in}}}$ in order to minimize the electronic to shot noise ratio. The optimal values of Δ are shown in Fig. 6b).

Performance analysis and comparisons with LLO-sequential. We have compared the expected key rates of the LLO-sequential and LLO-displacement designs as function of the repetition rate f and the results are plotted in Fig. 5. It represents the key rate as a function of the repetition rate for different lasers linewidths. In high phase noise regimes (low repetition rates), the LLO-sequential (dashed curves) can not produce secret key because the

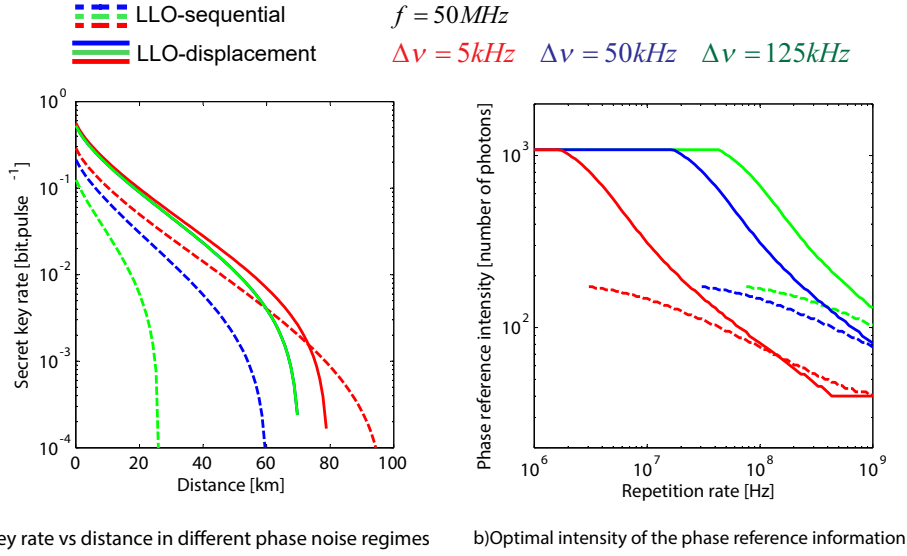


FIG. 6: (color) a) Secret key rate of both LLO-displacement and LLO-sequential designs as function of the distance in high phase noise regimes. b) Optimal intensity of the phase reference information in the LLO-displacement (displacement intensity) and in the LLO-sequential (phase reference intensity) as function of the repetition rate.

relative phase estimation efficiency is dominated by the noise V_{drift} from Eq. 11. However, when the repetition rate is high enough, the drift V_{drift} is small and phase correction is efficient. In contrast, in the LLO-displacement design, the phase noise can always be corrected due to systematic phase estimations. In low repetition rate regimes, the optimal phase estimation variance of Eq. 21 is the single-measurement based estimation while it can even be improved using the filtering technique in high repetition rates regimes. In low phase noise regimes, the phase noise is efficiently corrected in both designs and the gap between the curves come from the factor 1/2 which is saved in the LLO-displacement design due to simultaneous signal and phase reference transmission.

In Fig. 6a), we have plotted the expected secret key rates for both designs as function of the distance for different laser linewidths. The repetition rate is chosen to be $f = 50$ MHz. The blue and green solid curves (LLO-displacement) overlap and appear as a single solid curve. As expected, we can see that the LLO-displacement is much more resilient to large laser linewidths because the performances of LLO-sequential drastically drop with the increasing of the laser linewidths. Furthermore, we also can see that the LLO-sequential design allows to reach higher distances in low phase noise regimes because of the limit on the phase estimation efficiency due to finite AM dynamics. In the LLO-sequential, reference pulses however are fully dedicated to phase estimation. When $V_{\text{drift}} \approx 0$ (low phase noise regimes), the only noise contribution in the relative phase estimation from Eq. 12 is the shot noise. This implies that the required displacement amplitude has to be larger than the reference amplitude of LLO-sequential design. In Fig. 6b), we have plot theoretical optimal values, based on our simulations, for both the displacement amplitude in LLO-displacement and the reference pulse amplitude in LLO-sequential. First, we can see that E_{ref} is always smaller than Δ which results in a lower excess noise contribution of the AM leakage from Eq. 14. This gap in the AM excess noise allows the LLO-sequential design to reach longer distances in the regime of low phase noise as shown in Fig. 6a).

The single-measurement phase estimation variance V_M corresponds to the maximal remaining phase noise with which Bob can estimate the relative phase. In particular, if V_M is sufficiently low to allow a secret key generation, the LLO-displacement design can be used in any phase noise regime because of the self-coherence. We recall that the variance V_M is written as:

$$V_M = \frac{GV_A + 2}{G\Delta^2} \quad (25)$$

Thus, in order to ensure a low V_M , the number of photons Δ^2 should be large enough compared to $V_A + 2/G$. This can be ensured if the AM dynamics is sufficiently high. Inversely, for low phase noise regimes, the required displacement is smaller. As such, the minimal dynamics required to produce a secret key depends on the normalized phase noise which can be defined as the ratio $f/\Delta\nu$. We have plotted the theoretical expected achievable distance

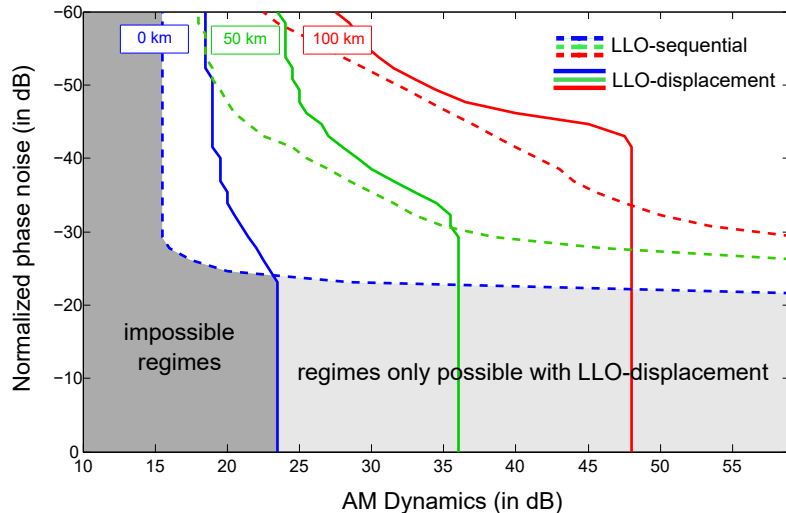


FIG. 7: (color) Experimental requirements in terms of amplitude modulator dynamics and phase noise regime to reach different distances: 0 km (blue curves), 50 km (green curves) and 100 km (red curves) with the LLO-sequential design (dashed curves) and the LLO-displacement design (solid curves). The dark grey region corresponds to impossible AM dynamics and phase noise regimes in both regimes. The light grey region corresponds to the phase noise/dynamics combinations allowing a secret key only with the LLO-displacement design (high phase noise regimes) at 0 km.

as a function of both the amplitude modulator dynamics and the phase noise for both the LLO-sequential and the LLO-displacement designs. The results are shown in Fig. 7. The dark grey region represents the regimes in which it is impossible to produce any secret key with both regimes. This basically corresponds to the low dynamics regimes in which no collective phase correction is possible and the AM leakage of Eq. 14 is large. This shows that the dynamics is a key parameter to allow LLO-based designs. The light grey region corresponds to high phase noise regimes in which it is possible to generate secret key using the LLO-displacement design but the phase drift the LLO-sequential design prevents any secret key generation. In particular, we can see that for any phase noise regime, there exists a minimal dynamics at which secret key generation is possible with the LLO-displacement. This means that every relative phase drift can be corrected provided a large enough displacement. This minimal dynamics increases with the distance because channel losses force to produce a higher displacement at emission which increases the modulation errors. Furthermore, the minimal dynamics decreases for low phase noise regime because the filtering algorithm allows to use lower displacements. From Fig. 7, we can see that there exists a phase noise threshold above which the minimal AM dynamics starts to decrease. This corresponds to the regime at which the filtering algorithm decreases the phase estimation below the single measurement phase noise variance V_M . This corresponds to the regime at which the optimal window size n_{opt} increases. From Eq. 11, we have:

$$n_{\text{opt}} > 0 \Leftrightarrow \frac{f}{\Delta\nu} > \frac{2\pi}{3V_M} = \frac{2\pi}{3} \cdot \frac{\Delta^2}{V_A + 2/G} \quad (26)$$

Inversely, in high phase regimes, the optimal phase estimation is V_M which does not depend on the phase noise regime but on the displacement Δ . A minimal dynamics of around 20 dB is then always required to ensure low enough modulation excess noise. We can also see from Fig. 7 that, in low phase noise regimes (normalized phase noise below 30 dB), the minimal dynamics required to allow secret key generation is lower in the LLO-sequential design (around 15 dB) than in the LLO-displacement design (around 20 dB). Basically, the intensity of LLO-sequential reference pulses has to be larger than the shot noise variance while the displacement intensity Δ^2 has to be larger than $V_A + 1$. This imposes higher Δ values than r_{ref} values and finally, the dynamics has to be larger in the LLO-displacement design. However, we emphasize that the required dynamics for high phase noise regimes, for instance 36 dB at 50 km, are compatible with standard AM dynamics with the LLO-displacement design.

In this section, we have then theoretically demonstrated the feasibility of a self-coherence reference phase sharing in CV-QKD while relying on standard equipment. In particular, the LLO-displacement design allows to perform CV-QKD in low cost hardware regimes while being strongly resilient to phase drift. As such, using the LLO-displacement design, emitter and LO can be realized with standard DFB lasers. This design lifts practical limitations of LLO-sequential designs and is a major step towards CV-QKD deployment.

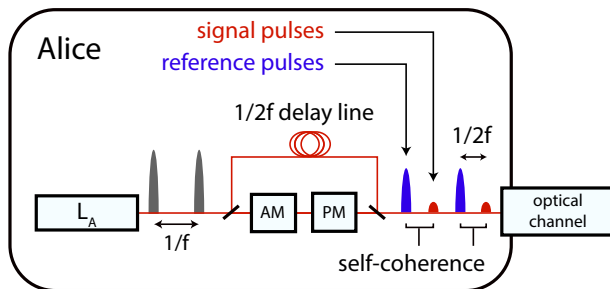


FIG. 8: (color) Experimental scheme of the LLO-delayline emitter. Laser pulses at repetition rate f are splitted using an unbalanced beamsplitter. The strong part is delayed using a $1/2f$ delay line while the weak part is modulated as the quantum signal. They are then recombined and sent through the optical channel at repetition rate $1/2f$.

In the next section, we introduce self-coherent derivations of the LLO-sequential design.

C. Delay line based self-coherent designs

In this section, we introduce a second family of self-coherent LLO designs in which quantum signal and phase reference are derived from the same laser pulse based on delay lines. This ensures a stable phase relation between signal and reference pulses and an efficient relative phase estimation is possible regardless of the phase noise regime. Furthermore, we propose two experimental receivers able to perform both signal measurement and phase correction based on the introduced emitter side. The first one, referred to as LLO-delayline-dsp, is based on digital signal processing (dsp) phase correction while the second, referred to as LLO-delayline-opll, relies on an optical phase-locking loop (opll). We show that theoretical performances of such designs are at least equivalent to those of the LLO-displacement although the overall performance might be hindered by the increased experimental complexity of realistic implementations.

1. The LLO-delay line emitter

We here introduce a design called LLO-delayline to derive pairs of self-coherent signal and phase reference pulses. The idea is here to use delay lines to derive pulse pairs with fixed relative phase hence a self-coherence property. Alice splits her laser output pulses (repetition rate f) into two parts using an unbalanced beamsplitter. The strong pulse is delayed of $1/2f$ second and used as the phase reference pulse while the weak one is modulated as the quantum signal pulse. The two pulses are then recombined and sent to Bob through the optical channel. After recombination, time between consecutive quantum signal and reference pulses is then $1/2f$. The ad-hoc phase coherence of the LLO-delayline can be outlined by noticing that, as output of the same laser pulse, quantum signal and phase reference both have a zero phase in Alice's reference frame. In other words, it can be expressed considering the differential phase θ_{diff}^A between quantum signal and phase reference from the same pair after recombination. As output of the same optical pulse, the phase θ_{diff}^A can be easily written in L_A 's reference frame as:

$$\theta_{\text{diff}}^A = \theta_{\text{state}} \quad (27)$$

which is the phase of the modulated coherent state from Eq. 5. In particular, the differential phase is a constant and does not depend on the laser phase drift. Thus, this is a self-coherence property.

The experimental scheme of the LLO-delayline emitter is detailed in Fig. 8. One advantage of this scheme is that the amplitude modulator does not modulate both signal and reference pulses which limits the constraints on AM dynamics. We now propose two experimental receiver schemes for this emitter scheme.

2. The LLO-delayline-dsp receiver

Bob receives consecutive pairs of self-coherent signal and reference pulses. In this receiver scheme, he uses a heterodyne detector to successively measure both quadratures of each received pulse. We show that, using digital

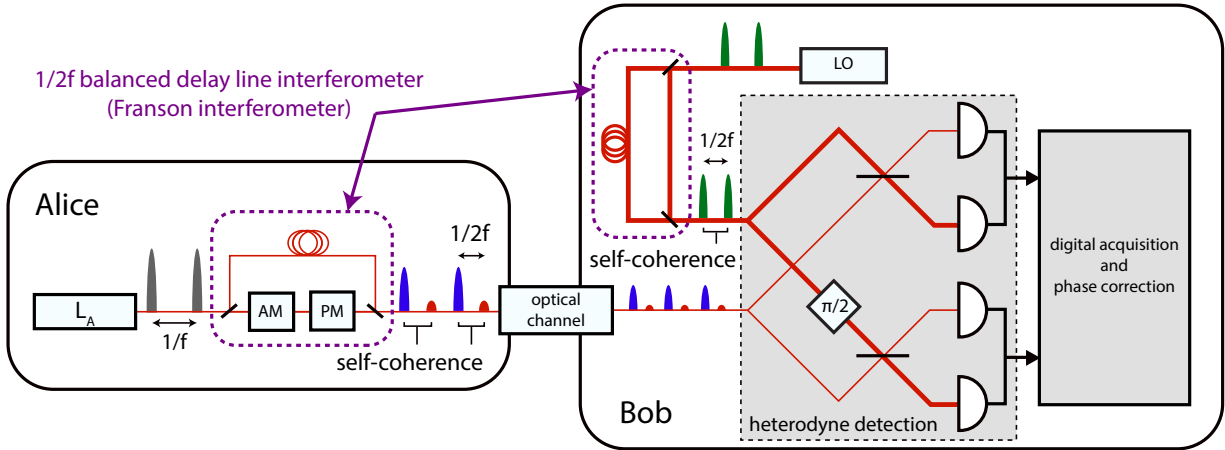


FIG. 9: (color) Full experimental scheme of the LLO-delayline-dsp design. Alice sends consecutive phase coherent signal/reference pulses pairs to Bob using the LLO-delayline emitter of Fig. 8. On his side, Bob uses his own laser as the LO for coherent detections using the same delay line technique to produce phase coherent LO pulses. Phase estimation and phase correction are digitally performed after measurement acquisition.

signal processing, he can both evaluate the relative phase noise and correct his measurements. Using the notations of the LLO-sequential phase noise analysis, we note θ_{2k} and θ_{2k+1} the relative phases between respectively quantum signal and phase reference pulse with corresponding LO pulses at interference. We emphasize that in order to maintain self-coherence after detection, Bob has to ensure a stable relation between θ_{2k} and θ_{2k+1} . As at emitter side, this can be done by producing self-coherent LO pulse pairs using a $1/2f$ delay line. The overall experimental scheme, shown in Fig. 9, can then be seen as a balanced Franson interferometer [34]. The differential phase $\theta_{\text{diff}}^{\text{LO}}$ between the two LO pulses of each pair is then set to 0 while the differential phase $\theta_{\text{diff}}^{\text{A}}$ between quantum signal and reference pulse is constant (Eq. 27). Finally, provided the interferometer is stable, the relative phase drift V_{drift} is equal to 0. Bob can then estimate the relative phase θ_{2k} with his phase estimation $\hat{\theta}_{2k+1}$ performed on the phase reference pulse. The variance of this estimate is expressed in Eq. 10 as:

$$V_M = \frac{2}{G \cdot E_{\text{ref}}^2} \quad (28)$$

Finally, using the expression of Eq. 12, the remaining relative phase noise using single pulse estimation is:

$$V_{\theta} = \frac{2}{G \cdot E_{\text{ref}}^2} \quad (29)$$

This scheme then automatically ensures a strong self-coherence at interference as, provided a stable delayline interferometer, the relative phase noise can be essentially removed. Bob gets self-coherent outcome measurements and is able to correct the phase drift in the same way as in the LLO-sequential design but with higher efficiency. Furthermore, the remaining phase noise does not depend on the phase noise regime. We however emphasize that delay lines have to be placed on both sides in order to ensure the phase coherence between two consecutive signal/reference and LO pairs. An important difficulty of this design is to ensure the required stability by perfectly balancing the two delay lines. In practice, even if the delay lines are perfectly balanced, the different optical path lengths fluctuate due to imperfect experimental conditions (temperature fluctuations for instance) which implies an imperfect balancing. In terms of phase noise, the LLO-delayline-dsp design is however slightly more performant than the LLO-displacement design because phase noise only comes from low frequency fluctuations on the experimental interferometer stability.

3. The LLO-delayline-opll receiver

We propose a second receiver for the LLO-delayline emitter scheme based on an optical phase-locking loop. At reception, Bob separates signal and phase reference pulses in two different optical paths using a polarization

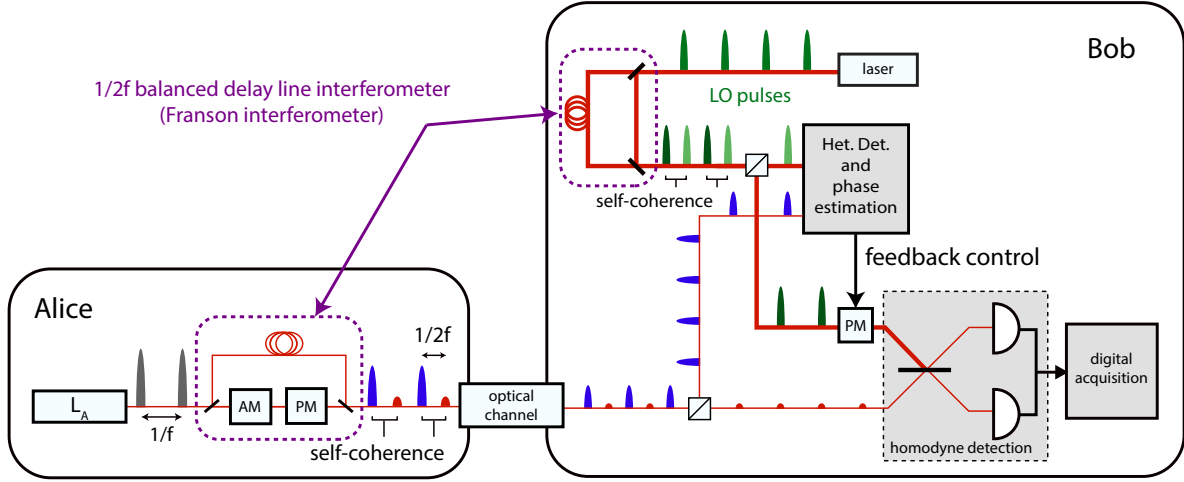


FIG. 10: (color) Full experimental scheme of the LLO-delayline-opp design. Alice sends consecutive phase coherent signal/reference pulses pairs to Bob using the LLO-delayline emitter of Fig. 8 with an additional polarization multiplexing for signal and phase reference. On his side, Bob uses a polarization beamsplitter to separate signal and phase reference pulses. Reference pulses are sent on the heterodyne detection for relative phase estimation. That estimation is used to feedback control the LO phase of the signal homodyne detection ensuring a physical phase coherence at interference.

beamsplitter. This requires an additional polarization multiplexing at emitter's side in order to be able to separate signal and reference pulses at Bob's side. At reception, signal and reference pulses are detected using different detections. Using a heterodyne detection to measure both quadrature of the reference pulses, Bob estimates the relative phase, cf. Eq. 28, while quantum signal pulses are detected using a homodyne detection. The phase estimate is then used to perform a feedback phase control on the LO of the signal homodyne detection. Doing this, a phase tracking is physically performed and the relative phase at interference of the quantum signal detection is controlled and phase coherence is physically ensured. This kind of design to dedicate a specific heterodyne detection for reference phase estimations and another coherent detection for quantum signal measurement.

In this experimental receiver scheme, detailed in Fig. 10, an important issue is the bandwidth of the feedback control which has to be larger than the repetition rate f . Furthermore, the overall remaining phase noise will depend on the performance of the optical phase-lock loop.

4. LLO-delayline performance and comparison with LLO-displacement.

The main challenge of LLO-delayline designs is related to its relative experimental complexity. Delay line interferometers as well as optical phase control require a very stable experimental setup. In practice, these additional experimental components may imply some additional technical noise on Bob's measurements due to imperfect balancings. In order to compare LLO-displacement and LLO-delayline-dsp designs, we introduce an additional technical noise threshold, of variance ξ_{add} in shot noise unit, which we define as the additional technical noise on the LLO-delayline-dsp designs at which the secret key rate of LLO-delayline-dsp and LLO-disp are equal. In other words, this is upper bound of tolerable additional noise to make the LLO-delayline-dsp more performant than LLO-displacement. In Fig. 11, we compare the secret key rates of the LLO-displacement and the LLO-delayline-dsp designs and also plot the additional noise threshold ξ_{add} . The key rate values are shown on the left axis while the excess noise values are shown on the right axis. At small distance, the LLO-displacement design is more performant than LLO-delayline. The difference between the key rates is dominated by a factor 2, in favor of the LLO-displacement design, since all pulses contribute to key generation. We can see that there exists a positive additional noise threshold ξ_{add} for long distances. This means that the LLO-delayline-dsp design allows higher key rates at long distance if a low enough technical noise is ensured. This is due to the systematic error in phase estimation in the LLO-displacement design due to finite ratio V_A/Δ^2 in Eq. 19. Furthermore, for low dynamics, the LLO-delayline allows a higher secret key rate because the constraints on the AM dynamics are relaxed (AM only modulates quantum signal). Finally, we can see that the threshold ξ_{add} is always relatively low which means that a low additional noise has to be ensured to make the LLO-delayline-dsp design competitive in

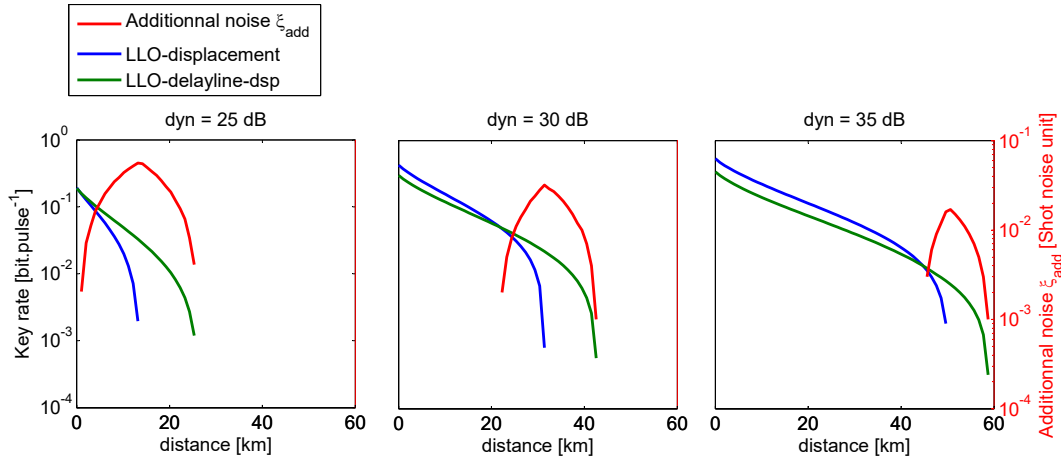


FIG. 11: (color) Comparison of the LLO-displacement and the LLO-delayline designs in term of secret key rates as function of the distance for three different dynamics (25 dB, 30 dB and 35 dB). Red curves correspond to the additional noise threshold ξ_{add} in shot noise unit.

term of secret key rate.

IV. CONCLUSION AND PERSPECTIVES

In order to reach long distance and lift security loophole issues, the local oscillator should not be directly sent through the optical channel in CV-QKD experiments. LLO-based CV-QKD protocols have been introduced. We have however shown that the only design proposed to date, the LLO-sequential design [1–3] requires to be used at low phase noise regimes ie. with expensive and very stable ECL lasers or with high repetition rates. An important issue of high repetition rate CV-QKD is the scaling of Bob’s detector electronic noise. For GHz CV-QKD, the electronic to shot noise ratio is about -1 dB even with efficient homodyne detector [18] which is a major obstacle to reach high repetition rates. In paranoid models [2] in which the electronic noise is supposed to be controlled by the eavesdropper, these values prevent any secret key generation. Using LLO-sequential design then requires expensive ultra low phase noise lasers and low electronic noise homodyne detectors which is a strong limitation. We have introduced new elements in the standard noise model of CV-QKD analysis taking into account new constraints imposed by the required simultaneous transmission of the quantum signal as well as a phase reference. In this work, we have introduced the idea of self-coherent phase correction scheme in CV-QKD protocols. This would allow to perform in high phase noise regime using low cost DFB lasers or working at low repetition rates provided large enough AM dynamics is available. For instance, in Fig. 7, we have shown that provided an AM dynamics of 47 dB would allow to reach 100 km even in high phase noise regime. This allows to perform LLO-based CV-QKD with standard equipment. Furthermore, our LLO-displacement design relies on a straightforward experimental setup and can be used in realistic regimes. We emphasize that to our knowledge the simultaneous quantum signal and phase reference transmission introduced in the LLO-displacement design is a new primitive which has not been studied so far in quantum communication regimes and can be applied to different signal modulation. Our results imply that next generation CV-QKD, implemented with a local LO, is possible even with low cost DFB lasers and standard AM. Such features are made possible by a self-coherent phase reference sharing design and are essential to progress towards photonics integration and wide deployment of CV-QKD.

-
- [1] Bing Qi, Pavel Lougovski, Raphael Pooser, Warren Grice, and Miljko Bobrek. Generating the local oscillator locally in continuous-variable quantum key distribution based on coherent detection. *Phys. Rev. X*, 5:041009, Oct 2015.
- [2] Daniel B. S. Soh, Constantin Brif, Patrick J. Coles, Norbert Lütkenhaus, Ryan M. Camacho, Junji Urayama, and Mohan Sarovar. Self-referenced continuous-variable quantum key distribution protocol. *Phys. Rev. X*, 5:041010, Oct 2015.

- [3] Duan Huang, Peng Huang, Dakai Lin, Chao Wang, and Guihua Zeng. High-speed continuous-variable quantum key distribution without sending a local oscillator. *Opt. Lett.*, 40(16):3695–3698, Aug 2015.
- [4] Valerio Scarani, Helle Bechmann-Pasquinucci, Nicolas J. Cerf, Miloslav Dušek, Norbert Lütkenhaus, and Momtchil Peev. The security of practical quantum key distribution. *Rev. Mod. Phys.*, 81:1301–1350, 2009.
- [5] Hoi-Kwong Lo, Marcos Curty, and Kiyoshi Tamaki. Secure quantum key distribution. *Nature Photonics*, 8:595–604, 2014.
- [6] www.secrenet.com.
- [7] www.idquantique.com.
- [8] Christian Weedbrook, Stefano Pirandola, Raúl García-Patrón, Nicolas J. Cerf, Timothy C. Ralph, Jeffrey H. Shapiro, and Seth Lloyd. Gaussian quantum information. *Rev. Mod. Phys.*, 84:621–669, May 2012.
- [9] Eleni Diamanti and Anthony Leverrier. Distributing secret keys with quantum continuous variables: Principle, security and implementations. *Entropy*, 17(9):6072, 2015.
- [10] M. Ziebell, M. Persechino, N. Harris, C. Galland, D. Marris-Morini, L. Vivien, E. Diamanti, and P. Grangier. Towards on-chip continuous-variable quantum key distribution. In *Conference on Lasers and Electro-Optics/European Quantum Electronics Conference (CLEO/Europe-EQEC)*, 2015.
- [11] Rupesh Kumar, Hao Qin, and Romain Alléaume. Coexistence of continuous variable QKD with intense dwdm classical channels. *New Journal of Physics*, 17:043027, 2015.
- [12] Yue-Meng Chi, Bing Qi, Wen Zhu, Li Qian, Hoi-Kwong Lo, Sun-Hyun Youn, A I Lvovsky, and Liang Tian. A balanced homodyne detector for high-rate gaussian-modulated coherent-state quantum key distribution. *New Journal of Physics*, 13(1):013003.
- [13] D Huang, J Fang, D Wang, P Huang, and G Zeng. A wideband balanced homodyne detector for high speed continuous-variable quantum key distribution systems. In *QCrypt*, 2013.
- [14] D. Lin D. Huang, P Huang and G. Zeng. Long-distance continuous-variable quantum key distribution by controlling excess noise. *Scientific Reports*, 6:19201, 2016.
- [15] Paul Jouguet, Sébastien Kunz-Jacques, and Anthony Leverrier. Long-distance continuous-variable quantum key distribution with a gaussian modulation. *Phys. Rev. A*, 84:062317, Dec 2011.
- [16] Stephen D. Bartlett, Terry Rudolph, and Robert W. Spekkens. Reference frames, superselection rules, and quantum information. *Rev. Mod. Phys.*, 79:555–609, 2007.
- [17] Kikuchi Kazuro. Fundamentals of coherent optical fiber communications. in *Journal of Lightwave Technology vol. 34, N°1*, 2016.
- [18] Duan Huang, Dakai Lin, Chao Wang, Weiqi Liu, Shuanghong Fang, Jinye Peng, Peng Huang, and Guihua Zeng. Continuous-variable quantum key distribution with 1 mbps secure key rate. *Opt. Express*, 23:17511–17519, 2015.
- [19] Paul Jouguet, Sébastien Kunz-Jacques, Anthony Leverrier, Philippe Grangier, and Eleni Diamanti. Experimental study on the gaussian-modulated coherent-state quantum key distribution over standard telecommunication fibers. *Nature Photonics*, 7:378–381, 2013.
- [20] Bing Qi, Lei-Lei Huang, Li Qian, and Hoi-Kwong Lo. Experimental study on the gaussian-modulated coherent-state quantum key distribution over standard telecommunication fibers. *Phys. Rev. A*, 76:052323, Nov 2007.
- [21] A. Ferenczi, P. Grangier, and F. Grosshans. Calibration attack and defense in continuous variable quantum key distribution. In *Lasers and Electro-Optics, 2007 and the International Quantum Electronics Conference. CLEOE-IQEC 2007. European Conference on*, pages 1–1, June 2007.
- [22] Xiang-Chun Ma, Shi-Hai Sun, Mu-Sheng Jiang, Ming Gui, Yan-Li Zhou, and Lin-Mei Liang. Enhancement of the security of a practical continuous-variable quantum-key-distribution system by manipulating the intensity of the local oscillator. *Phys. Rev. A*, 89:032310, Mar 2014.
- [23] Paul Jouguet, Sébastien Kunz-Jacques, and Eleni Diamanti. Preventing calibration attacks on the local oscillator in continuous-variable quantum key distribution. *Phys. Rev. A*, 87:062313, Jun 2013.
- [24] Jing-Zheng Huang, Christian Weedbrook, Zhen-Qiang Yin, Shuang Wang, Hong-Wei Li, Wei Chen, Guang-Can Guo, and Zheng-Fu Han. Quantum hacking of a continuous-variable quantum-key-distribution system using a wavelength attack. *Phys. Rev. A*, 87:062329, Jun 2013.
- [25] Frédéric Grosshans and Philippe Grangier. Continuous variable quantum cryptography using coherent states. *Phys. Rev. Lett.*, 88:057902, 2002.
- [26] Raul Garcia-Patron. Quantum information with optical continuous variables : from bell tests to key distribution. 2008.
- [27] Simon Fossier. Mise en oeuvre et évaluation de dispositifs de cryptographie quantique à longueur d’onde télécom. 2009.
- [28] Yasuhiro Aoki, Kasuhito Tajima, and Ikuo Mito. Input power limits of single-mode optical fibers due to stimulated brillouin scattering in optical communication systems. *Journal of Lightwave Technology*, 6, 1988.
- [29] Kaoru Shimizu, Tsuneo Horiguchi, Yahei Koyamada, and Toshio Kurashima. Coherent self-heterodyne detection of spontaneously brillouin-scattered light waves in a single-mode fiber. *Opt. Lett.*, 18(3):185–187, 1993.
- [30] Govind P Agrawal. *Nonlinear fiber optics*. Academic press, 2007.
- [31] Theresa A Maldonado. Electro-optic modulators. *Handbook of optics*, 2, 1995.
- [32] Paul Jouguet, Sébastien Kunz-Jacques, Eleni Diamanti, and Anthony Leverrier. Analysis of imperfections in practical continuous-variable quantum key distribution. *Phys. Rev. A*, 86:032309, Sep 2012.
- [33] Hao Qin, Rupesh Kumar, and Romain Alléaume. Quantum hacking: Saturation attack on practical continuous-variable quantum key distribution. *arXiv:1511.01007*, 2015.
- [34] J. D. Franson. Bell inequality for position and time. *Phys. Rev. Lett.*, 62:2205–2208, May 1989.

V. ANNEX

A. Secret key rate formulas for CV-QKD

In this work, we focus on the Gaussian-modulated coherent state (GMCS) protocol [25]. In GMCS, Alice encodes zero-mean gaussian classical variables x_A and p_A on both the \hat{x} and \hat{p} quadratures of coherent states [8] before sending them to Bob through an insecure optical channel controlled by an eavesdropper Eve. At reception, Bob measures either one of the quadratures (\hat{x} for instance but has to be randomly chosen) using a homodyne detection or both quadrature using a heterodyne detection and gets a value x_B . Throughout this paper, we have considered that Eve's behaviour is captured under the collective attacks model. Thus, we can express the expected key rate k for reverse reconciliation as [4]:

$$k = \beta I_{AB} - \chi_{BE} \quad (30)$$

where I_{AB} is the mutual information between Alice's variable and Bob's measurements, β is the efficiency of the reconciliation algorithm and χ_{BE} is Eve's maximal accessible information on Bob's measurements which is the Holevo information for collective attacks. In the following, we detail the secret key formulas [27] we have used in this work.

a. Secret key formulas for homodyne receiver. For a homodyne detection, we can write:

$$I_{AB}^{\text{hom}} = \frac{1}{2} \cdot \log_2 \left(\frac{V_A + 1 + \chi_{\text{tot}}}{1 + \chi_{\text{tot}}} \right) \quad (31)$$

where:

$$\chi_{\text{tot}} = \chi_{\text{line}} + \frac{\chi_{\text{hom}}}{T} \quad ; \quad \chi_{\text{line}} = \frac{1-T}{T} + \xi_{\text{line}} \quad ; \quad \chi_{\text{hom}} = \frac{1-\eta}{\eta} + \xi_{\text{hom}} \quad (32)$$

$$(33)$$

and

$$\chi_{BE} = G\left(\frac{\lambda_1 - 1}{2}\right) + G\left(\frac{\lambda_2 - 1}{2}\right) - G\left(\frac{\lambda_3 - 1}{2}\right) - G\left(\frac{\lambda_4 - 1}{2}\right) \quad (34)$$

where

$$G(x) = (x+1) \cdot \log_2(x+1) - x \cdot \log_2(x) \quad (35)$$

$$\lambda_{1,2}^2 = \frac{1}{2} \cdot (A \pm \sqrt{A^2 - 4B}) \quad (36)$$

$$\lambda_{3,4}^2 = \frac{1}{2} \cdot (C \pm \sqrt{C^2 - 4D}) \quad (37)$$

$$A = V^2(1-2T) + 2T + T^2(V + \chi_{\text{line}})^2 \quad (38)$$

$$B = T^2(V\chi_{\text{line}} + 1)^2 \quad (39)$$

$$C = \frac{V\sqrt{B} + T(V + \chi_{\text{line}}) + A\chi_{\text{hom}}}{T(V + \chi_{\text{tot}})} \quad (40)$$

$$D = \sqrt{B} \cdot \frac{V + \sqrt{B}\chi_{\text{hom}}}{T(V + \chi_{\text{tot}})} \quad (41)$$

b. Secret key formulas for heterodyne receiver. For a heterodyne detection, we can write:

$$I_{AB}^{\text{het}} = \log_2 \left(\frac{V_A + 1 + \chi_{\text{tot}}}{1 + \chi_{\text{tot}}} \right) \quad (42)$$

where:

$$\chi_{\text{tot}} = \chi_{\text{line}} + \frac{\chi_{\text{het}}}{T} \quad ; \quad \chi_{\text{line}} = \frac{1-T}{T} + \xi_{\text{line}} \quad ; \quad \chi_{\text{het}} = \frac{2-\eta}{\eta} + 2\xi_{\text{het}} \quad (43)$$

$$(44)$$

and

$$\chi_{\text{BE}} = G\left(\frac{\lambda_1 - 1}{2}\right) + G\left(\frac{\lambda_2 - 1}{2}\right) - G\left(\frac{\lambda_3 - 1}{2}\right) - G\left(\frac{\lambda_4 - 1}{2}\right) \quad (45)$$

where

$$G(x) = (x + 1) \cdot \log_2(x + 1) - x \cdot \log_2(x) \quad (46)$$

$$\lambda_{1,2}^2 = \frac{1}{2} \cdot (A \pm \sqrt{A^2 - 4B}) \quad (47)$$

$$\lambda_{3,4}^2 = \frac{1}{2} \cdot (C \pm \sqrt{C^2 - 4D}) \quad (48)$$

$$A = V^2(1 - 2T) + 2T + T^2(V + \chi_{\text{line}})^2 \quad (49)$$

$$B = T^2(V\chi_{\text{line}} + 1)^2 \quad (50)$$

$$C = \frac{A\chi_{\text{het}}^2 + B + 1 + 2\chi_{\text{het}}(V\sqrt{B} + T(V + \chi_{\text{line}})) + 2T(V^2 - 1)}{(T(V + \chi_{\text{tot}}))^2} \quad (51)$$

$$D = \left(\frac{V + \sqrt{B}\chi_{\text{hom}}}{T(V + \chi_{\text{tot}})}\right)^2 \quad (52)$$

B. Excess noise calculations

1. Excess noise due to phase noise

Alice sends the coherent state $|\alpha\rangle = |x_A + \Delta, p_A\rangle$. For simplicity, we consider channel loss and relative phase noise as the only excess noise source in this analysis. Due to channel loss and relative phase drift θ , Bob receives the coherent state $\sqrt{G/2} \cdot |e^{-i\theta}\alpha\rangle$. As such, Bob gets the following measurement outcomes $(\tilde{x}_B, \tilde{p}_B)$:

$$\begin{pmatrix} \tilde{x}_B \\ \tilde{p}_B \end{pmatrix} = \sqrt{\frac{G}{2}} \cdot \begin{pmatrix} \cos \theta & \sin \theta \\ -\sin \theta & \cos \theta \end{pmatrix} \cdot \begin{pmatrix} x_A + \Delta \\ p_A \end{pmatrix} + \begin{pmatrix} x_0 \\ p_0 \end{pmatrix} \quad (53)$$

where (x_0, p_0) the vacuum quadratures. We suppose that Bob gets an estimator $\hat{\theta} \sim \mathcal{N}(\theta, V_{\hat{\theta}})$. He can then estimate Alice's quadrature as:

$$\begin{pmatrix} x_B \\ p_B \end{pmatrix} = \sqrt{\frac{2}{G}} \cdot \begin{pmatrix} \cos \hat{\theta} & -\sin \hat{\theta} \\ \sin \hat{\theta} & \cos \hat{\theta} \end{pmatrix} \cdot \begin{pmatrix} \tilde{x}_B \\ \tilde{p}_B \end{pmatrix} - \begin{pmatrix} \Delta \\ 0 \end{pmatrix} \quad (54)$$

which can be simplified by denoting $\bar{\theta} = \hat{\theta} - \theta$ as the remaining phase noise. By construction, it verifies $\bar{\theta} \sim \mathcal{N}(0, V_{\bar{\theta}})$. We can then write Eq. 54 as:

$$\begin{pmatrix} x_B \\ p_B \end{pmatrix} = \begin{pmatrix} \cos \bar{\theta} & -\sin \bar{\theta} \\ \sin \bar{\theta} & \cos \bar{\theta} \end{pmatrix} \cdot \begin{pmatrix} x_A + \Delta \\ p_A \end{pmatrix} + \sqrt{\frac{2}{G}} \cdot \begin{pmatrix} \cos \hat{\theta} & -\sin \hat{\theta} \\ \sin \hat{\theta} & \cos \hat{\theta} \end{pmatrix} \cdot \begin{pmatrix} x_0 \\ p_0 \end{pmatrix} - \begin{pmatrix} \Delta \\ 0 \end{pmatrix} \quad (55)$$

Finally, we can calculate the variance of the noise of Bob's estimator as:

$$\text{var}(x_B - x_A) = \text{var} \left((x_A + \Delta) \cdot \cos \bar{\theta} - p_A \cdot \sin \bar{\theta} + \sqrt{\frac{2}{G}} \cdot (x_0 \cdot \cos \hat{\theta} - p_0 \cdot \sin \hat{\theta}) - \Delta - x_A \right) \quad (56)$$

$$= \text{var} \left(x_A \cdot (1 - \cos \bar{\theta}) + \Delta \cdot \cos \bar{\theta} - p_A \cdot \sin \bar{\theta} \right) + \frac{2}{G} \cdot \text{var} \left(x_0 \cdot \cos \hat{\theta} - p_0 \cdot \sin \hat{\theta} \right) \quad (57)$$

$$= \frac{2}{G} + \text{var} \left[x_A \cdot (1 - \cos \bar{\theta}) \right] + \text{var} \left[p_A \cdot \sin \bar{\theta} \right] + \text{var} \left[\Delta \cdot \cos \bar{\theta} \right] \quad (58)$$

$$= \frac{2}{G} + V_A \cdot \left(\mathbb{E} \left[(1 - \cos \bar{\theta})^2 \right] + \mathbb{E} \left[\sin^2 \bar{\theta} \right] \right) + \Delta^2 \cdot \text{var} \left(\cos \bar{\theta} \right) \quad (59)$$

$$= \frac{2}{G} + 2 \cdot V_A \cdot (1 - e^{-V_{\bar{\theta}}}) + \Delta^2 \cdot \left(\frac{1}{2} + \frac{1}{2} e^{-2V_{\bar{\theta}}} - e^{-V_{\bar{\theta}}} \right) \quad (60)$$

The first term corresponds to the channel loss induced noise while the remaining part results in the Eq. 23 and Eq. 8 for $\Delta = 0$.